

# PHYSICS-INFORMED GNN FOR MEDIUM-HIGH VOLTAGE AC POWER FLOW WITH EDGE-AWARE ATTENTION AND LINE SEARCH CORRECTION OPERATOR

Changhun Kim<sup>1</sup>, Timon Conrad<sup>2</sup>, Redwanul Karim<sup>1</sup>, Julian Oelhaf<sup>1</sup>, David Riebesel<sup>2</sup>,  
Tomás Arias-Vergara<sup>1</sup>, Andreas Maier<sup>1</sup>, Johann Jäger<sup>2</sup>, Siming Bayer<sup>1</sup>

<sup>1</sup> Pattern Recognition Lab, Friedrich-Alexander-Universität Erlangen-Nürnberg, Germany

<sup>2</sup> Institute of Electrical Energy Systems, Friedrich-Alexander-Universität Erlangen-Nürnberg, Germany

## ABSTRACT

Physics-informed graph neural networks (PIGNNs) have emerged as fast AC power-flow solvers that can replace the classic Newton–Raphson (NR) solvers, especially when thousands of scenarios must be evaluated. However, current PIGNNs still need accuracy improvements at parity speed; in particular, the physics loss is inoperative at inference, which can deter operational adoption. We address this with PIGNN-Attn-LS, combining an edge-aware attention mechanism that explicitly encodes line physics via per-edge biases, capturing the grid’s anisotropy, with a backtracking line-search based globalized correction operator that restores an operative decrease criterion at inference. Training and testing use a realistic High-/Medium-Voltage scenario generator, with NR used only to construct reference states. On held-out HV cases consisting of 4–32-bus grids, PIGNN-Attn-LS achieves a test RMSE of 0.00033 p.u. in voltage and 0.08° in angle, outperforming the PIGNN-MLP baseline by 99.5% and 87.1%, respectively. With streaming micro-batches, it delivers 2–5× faster batched inference than NR on 4–1024-bus grids.

**Index Terms**— AC power flow, physics-informed neural networks, graph neural networks, backtracking line search, power systems

## 1. INTRODUCTION

AC Power Flow (PF) computes bus voltages and angles that are consistent with network physics. It serves as a cornerstone for critical operational and planning tasks, including security assessment and optimization tasks [1–3]. In real-world practice, system operators must repeatedly solve AC-PF across large scenario sets spanning both High Voltage (HV) and Medium Voltage (MV) grids. This creates two central requirements: robust convergence across diverse operating conditions and high computational throughput for large-scale scenario evaluation.

State of the practice PF solvers only partly meet these needs. Newton–Raphson (NR) often converges rapidly when well initialized, but calculating inverse of Jacobian via sparse triangular solves is not naturally GPU-friendly [4]. Fast-decoupled load flow (FDLF) is quicker but relies on reactance dominant, weak-coupling assumptions and loses accuracy when those assumptions break [5]. In both approaches, performance hinges on large sparse linear systems

Corresponding author: changhun.kim@fau.de. This work was conducted within the scope of the research project *GridAssist* and was supported through the “OptiNetD” funding initiative by the German Federal Ministry for Economic Affairs and Energy (BMWE) as part of the 8<sup>th</sup> Energy Research Programme.

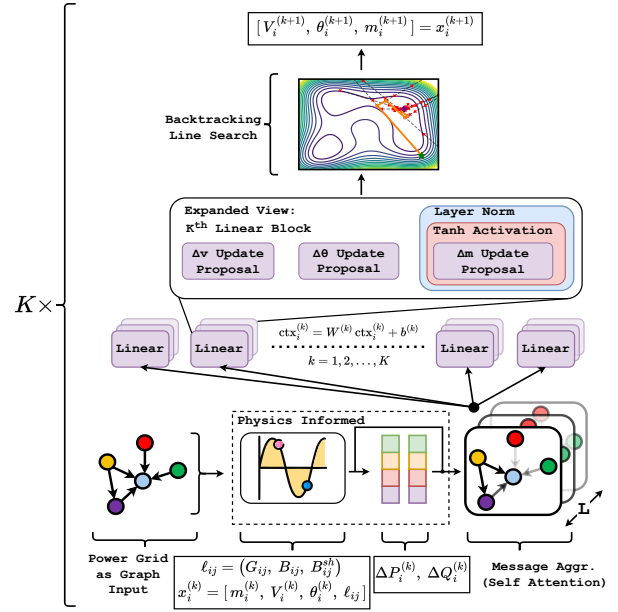


**Fig. 1.** Architecture of PIGNN-Attn-LS. Message aggregation uses  $L$  layers of edge-aware multi-head self-attention and is interchangeable with an MLP. The central node denotes the bus of interest; incoming edges are weighted by attention scores, with lower opacity indicating lower importance.

where cost worsen with network size and conditioning [6], creating a brittle accuracy–speed trade-off: improving the robustness of the solver often slows it down, whereas making it fast typically degrades accuracy.

Plain ML/DL surrogates [1] are fast but tied to a fixed topology and therefore do not scale, while graph-based GNN surrogates [7] transfer across sizes and layouts, but are typically not physics-informed because they imitate NR outputs. In contrast, Physics-informed graph neural networks (PIGNNs) combine physics guidance with graph scalability: they model the grid as a graph and learn a residual-to-update operator that maps power-mismatch signals  $\Delta P$  and  $\Delta Q$  to voltage–angle corrections via message passing, making them a strong choice for large, variable grids.

Trained with physics losses rather than NR labels, PIGNNs amortize computation over scenarios, preserve inductive biases from

Kirchhoff's laws, and can generalize across grid sizes. Properly designed, a PIGNN behaves like a learned inverse Jacobian, producing corrections that either (i) solve AC-PF directly or (ii) warm-start NR so that only a few Newton steps are needed, maintaining NR precision while reducing wall time.

Prior PIGNN research has established a strong foundation along three practical lines: (i) *end-to-end physics-informed solvers*, where unrolled message passing trained on residual penalties delivers high throughput with modest memory, spanning node-centric and bidirectional node/edge updates to shallow GCNs [8–14]; (ii) *stronger physics or hybrid constraints*, in which physics-guided decoders and augmented-Lagrangian objectives tighten the learning signal and accommodate uncertain admittances and mixed AC/DC grids within a single pipeline [15, 16]; and (iii) *warm starts for numerical optimization*, where learned initializers reduce downstream iterations; RL- and GNN-based warm starts shorten Newton steps and accelerate optimal power flow on various benchmarks [7, 17, 18].

Building on this foundation, the pursuit of accuracy at parity speed remains a central research direction, with several proposed architectures and training strategies emerging in the literature. On the architectural side, many GNN variants, especially attention-based methods [19, 20], have been explored; however, two limitations persist: (i) edge physics are encoded only implicitly through node embeddings, and (ii) training relies on NR labels. To address these issues, *we propose an edge-aware attention mechanism* tailored to a physics-informed architecture; each head is biased by admittance features, producing sharper, physics-faithful message weights.

Beyond architectural design, another limitation of existing PIGNNs is that the physics loss guiding training remains inoperative during inference, leaving the forward unroll without a built-in convergence guarantee on out-of-distribution cases. To provide inference-time globalization, *we incorporate a backtracking line search* [21] on a merit function to adaptively select the step size for the  $K$  message-passing updates in  $(\Delta V, \Delta \theta)$ , guaranteeing sufficient decrease of the merit at each iteration.

For evaluating the proposed model, the choice of data is crucial. Although various benchmark power grid data sets [22, 23] and synthetic data generation methods [24] have recently been released, *we build our own scenario synthesis pipeline* designed to better reflect European and German grids.

Finally, *we analyze throughput* in single-case and multi-scenario settings, comparing CPU Newton–Raphson (multiprocessing) with GPU PIGNN using streaming micro-batches. We report median inference over warm-up and repeated runs and identify the problem-size regimes where PIGNN surpasses NR.

Code: [github.com/Kimchangheon/PIGNN-Attn-LS](https://github.com/Kimchangheon/PIGNN-Attn-LS)

## 2. METHODOLOGY

### 2.1. Problem Formulation

We model the grid as an undirected graph  $\mathcal{G} = (\mathcal{V}, \mathcal{E})$  with  $N = |\mathcal{V}|$  buses. The node state is complex voltage  $x = [V, \theta] \in \mathbb{R}^{2N}$ , where  $V = |V|$  and  $\underline{V} = V \cdot e^{j\theta}$ . Currents are  $\underline{I} = \underline{Y} \cdot \underline{V}$  with  $\underline{Y} \in \mathbb{C}^{N \times N}$  and complex powers  $\underline{S} = \underline{V} \cdot \underline{I}^*$ , giving  $P = \Re\{\underline{S}\}$  and  $Q = \Im\{\underline{S}\}$ . For setpoints  $(P^{\text{set}}, Q^{\text{set}})$ , define residuals

$$\Delta P = P^{\text{set}} - P, \quad \Delta Q = Q^{\text{set}} - Q.$$

Classical Newton–Raphson solves PF by computing the step  $\Delta x = -J(x)^{-1}r(x)$  for  $r(x^*) = 0$ , where

$$r(x) = \begin{bmatrix} \Delta P \\ \Delta Q \end{bmatrix}, \quad J = \begin{bmatrix} \frac{\partial P}{\partial \theta} & \frac{\partial P}{\partial V} \\ \frac{\partial Q}{\partial \theta} & \frac{\partial Q}{\partial V} \end{bmatrix} = \begin{bmatrix} H & N \\ M & L \end{bmatrix}.$$

$J$  depends nonlinearly on admittances, voltages, and angle differences; building and solving it is expensive on large meshed grids. [25]

Instead, we learn a graph-structured residual-to-update operator

$$\Delta x \approx \mathcal{G}_\theta(x, Y) r(x),$$

### 2.2. Unrolling $K$ Correction Steps

We unroll  $K$  iterative correction steps of message passing over  $\mathcal{G}$ , producing a sequence  $\{x^{(k)}\}_{k=0}^K$ . At each step  $k$ , we compute mismatch residuals  $(\Delta P^{(k)}, \Delta Q^{(k)})$ , exchange messages among neighboring nodes, and propose updates  $(\Delta \theta^{(k)}, \Delta V^{(k)})$ . The generic update at node  $i$  is :

$$m_i^{(k+1)} = \text{UPDATE}^{(k)}\left(m_i^{(k)}, \Phi_{\text{phys}}^{(k)}\left(\text{AGGREGATE}^{(k)}\left(\{m_j^{(k)} \mid j \in \mathcal{N}(i)\}, \text{state}^{(k)}\right)\right)\right). \quad (1)$$

where  $\Phi_{\text{phys}}^{(k)}$  injects the residuals into the node features, forming a physically grounded learning signal that guides the neural solver toward satisfying the AC–PF equations in 2.1. Accordingly, training minimizes a discounted sum of stepwise-mismatch penalties over the unrolled iterations, with discount factor  $\gamma \in (0, 1]$ :

$$\mathcal{L}_{\text{phys}} = \sum_{k=0}^{K-1} \gamma^{K-1-k} \frac{1}{N} \sum_{i=1}^N [(\Delta P_i^{(k)})^2 + (\Delta Q_i^{(k)})^2].$$

Building on this idea, we construct a baseline, PIGNN-MLP, which follows the Graph Neural Solver paradigm [8] and uses an multi-layer perceptron (MLP) message aggregator in the DeepSets sense [26]. This choice makes neighbor aggregation permutation invariant and, despite its simplicity, yields competitive performance. Nevertheless, the resulting operator behaves as a stationary, isotropic graph filter. However, AC power-flow sensitivities are state dependent, directional, and strongly influenced by the line admittances  $Y_{ij}$ . Uniform aggregation therefore cannot emulate the anisotropic structure of  $J(x)^{-1}$ , motivating a more expressive, physics-aware formulation.

### 2.3. Physics-Informed, Edge-Aware Multi-Head Self-Attention

To overcome the limitations of isotropic MLP aggregation, we adopt a Transformer-style [27], edge-aware multi-head self-attention aggregator. The physics-informed node features by  $\Phi_{\text{phys}}^{(k)}$  at iteration  $k$ ,  $x_i^{(k)} = [V_i^{(k)}, \theta_i^{(k)}, \Delta P_i^{(k)}, \Delta Q_i^{(k)}, m_i^{(k)}] \in \mathbb{R}^{4+d}$ , we then form queries, keys, and values at step  $k$ . For each undirected edge  $(i, j) \in \mathcal{E}$ , we consider both scored directions  $j \rightarrow i$  and  $i \rightarrow j$ . For head  $h = 1, \dots, H$  with per-head dimensionality  $d_h = d_{\text{model}}/H$ ,

$$q_i^{(h)} = W_Q^{(h)} x_i^{(k)}, \quad k_j^{(h)} = W_K^{(h)} x_j^{(k)}, \quad v_j^{(h)} = W_V^{(h)} x_j^{(k)}.$$

The attention score is computed as a softmax over the neighbors

$$\alpha_{ij}^{(h)} = \text{softmax}\left(\frac{\langle q_i^{(h)}, k_j^{(h)} \rangle}{\sqrt{d_h}} + \beta_{ij}^{(h)}\right), \quad \beta_{ij}^{(h)} = f_{\text{edge}}^{(h)}(\ell_{ij})$$

and the multi-head aggregated context delivered to node  $i$  is:

$$\text{ctx}_i^{(k)} = W_O \left[ \sum_j \alpha_{ij}^{(1)} v_j^{(1)} \parallel \dots \parallel \sum_j \alpha_{ij}^{(H)} v_j^{(H)} \right] \in \mathbb{R}^d.$$

The edge-dependent bias  $\beta_{ij}^{(h)}$  injects admittance features directly into the attention scores, yielding a strong line-physics inductive bias; by contrast, MLP or standard graph attention network [28] aggregation incorporates admittance only implicitly via node features  $\Delta P, \Delta Q$ .

Leveraging this explicit encoding of line physics, the mechanism (i) yields a state-dependent, non-stationary propagation operator  $\Pi_h[i, j] = \alpha_{ij}^{(h)}(x, Y)$  that can approximate the local inverse-Jacobian action  $\Delta x \approx \mathcal{G}_\theta(x, Y) r$  more faithfully than uniform aggregators; (ii) by duplicating each undirected edge into two scored directions, it allows  $\alpha_{ij} \neq \alpha_{ji}$ , matching the directionality in the Jacobian blocks ( $H \neq H^\top$  in general); (iii) the multi-head structure lets different heads specialize to, for example, conductive vs. susceptible couplings, forming a low-rank, block-structured approximation to  $J(x)^{-1}$ ; and (iv) stacking  $L$  attention layers per iteration yields within-iteration multi-hop context without increasing  $K$ . Conceptually and empirically, this physics-aware attention improves power-flow learning relative to uniform aggregation.

#### 2.4. Backtracking line search and Voltage update caps

In nonlinear optimization, globalization techniques such as backtracking line search [21] enforce descent by adaptively selecting the step size to guarantee a sufficient decrease of a merit function. To compensate for the inoperative physics loss at inference, we apply a backtracking line search at each message-passing iteration  $k$  using the power-mismatch merit function. This restores an operative decrease criterion during inference and improves stability. The detailed procedure appears in Algorithm 1. In addition, we enforce per-iteration step caps and voltage bounds to promote monotonic decrease and to keep states within realistic operating ranges.

---

##### Algorithm 1: Backtracking Line Search with Update Caps

---

**Input** : Current state  $(\theta^{(k)}, V^{(k)}, m^{(k)})$ ;  
proposed updates  $(\Delta\theta^{(k)}, \Delta V^{(k)}, \Delta m^{(k)})$ ;  
constants  $c_1, \rho, \alpha_{\min}, d_\theta^{\max}, d_v^{\text{frac}}, V_{\min}, V_{\max}$ .  
**Output**: Updated state  $(\theta^{(k+1)}, V^{(k+1)}, m^{(k+1)})$ .  
**Merit function**:  
 $F(V, \theta) = \max\{\|\Delta P(V, \theta)\|_\infty, \|\Delta Q(V, \theta)\|_\infty\}$ ;  
Clip  $\Delta\theta^{(k)}$  and  $\Delta V^{(k)}$  to per-step caps  
 $|\Delta\theta^{(k)}| \leq d_\theta^{\max}, |\Delta V^{(k)}| \leq d_v^{\text{frac}} V^{(k)}$ ;  
Ensure state within bounds:  
 $\theta^{(k)} \leftarrow \text{wrap}(\theta^{(k)}), V^{(k)} \leftarrow \text{clip}(V^{(k)})$ ;  
Initialize  $\alpha \leftarrow 1$ ; set  $F_k \leftarrow F(V^{(k)}, \theta^{(k)})$ ;  
**while**  
 $F(\text{clip}(V^{(k)} + \alpha \Delta V^{(k)}), \text{wrap}(\theta^{(k)} + \alpha \Delta\theta^{(k)})) >$   
 $(1 - c_1 \alpha) F_k$  **do**  
 $\alpha \leftarrow \rho \alpha$ ; // Backtrack  
**if**  $\alpha < \alpha_{\min}$  **then**  
 $\alpha \leftarrow \alpha_{\min}$  **break**  
**if**  $\alpha \geq \alpha_{\min}$  **or**  
 $F(\text{clip}(V^{(k)} + \alpha_{\min} \Delta V^{(k)}), \text{wrap}(\theta^{(k)} + \alpha_{\min} \Delta\theta^{(k)})) <$   
 $F_k$  **then**  
 $\theta^{(k+1)} = \text{wrap}(\theta^{(k)} + \alpha \Delta\theta^{(k)}), V^{(k+1)} =$   
 $\text{clip}(V^{(k)} + \alpha \Delta V^{(k)}), m^{(k+1)} = m^{(k)} + \alpha \Delta m^{(k)}$ ;  
**else**  
 $\theta^{(k+1)} = \theta^{(k)}, V^{(k+1)} = V^{(k)}, m^{(k+1)} = m^{(k)}$ ;

---

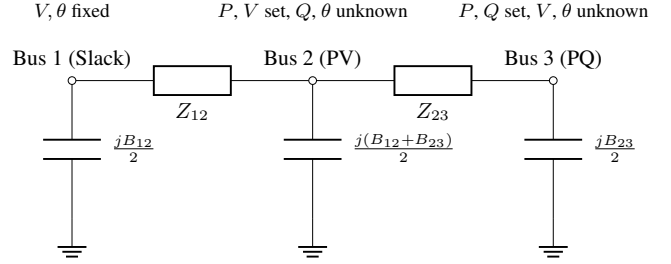


**Fig. 2.** Three-bus  $\pi$ -model (series  $R+jX$ ; half shunt per line end).  $Z_{ij} = (R' + jX')L_{ij}$ ,  $y_{ij} = 1/Z_{ij}$ ,  $B_{ij}^{\text{sh}} = \omega C' L_{ij}$  (total per line, split as  $B_{ij}^{\text{sh}}/2$  at each end);  $B_i^{\text{sh}} = \frac{1}{2} \sum_{j \in \mathcal{N}(i)} B_{ij}^{\text{sh}}$ . Admittance matrix:  $Y_{ij} = -y_{ij}$  on lines and  $Y_{ii} = \sum_{k \in \mathcal{N}(i)} y_{ik} + jB_i^{\text{sh}}$ .

### 3. SCENARIO SYNTHESIS AND REFERENCE POWER-FLOW SOLUTIONS (MV & HV)

Guided by Europe/Germany–typical overhead-line parameter ranges (Table 1) for series impedance and shunt charging [29–31], we synthesize physically plausible MV/HV grids, instantiating each line with a  $\pi$ -model; the series and shunt terms are indicated in Fig. 2. For each case, we draw a connected topology with one Slack bus and the remaining buses typed as PV or PQ, and we sample operating injections  $(P_i^{\text{set}}, Q_i^{\text{set}})$  by regime. Initial voltages  $V^{(0)}$  use magnitudes in  $[0.9, 1.1]$  p.u. for Slack and PV buses and 1.0 p.u. for PQ buses, with zero angle; conversion to engineering units follows  $V_{\text{base}}$ . We then compute a reference solution by running NR for up to  $K$  iterations on  $(Y, S^{\text{set}})$  under Slack/PV/PQ constraints to obtain  $(V^*, S^*)$ . Non-convergent or disconnected draws are discarded. MV cases emphasize higher  $R/X$  and shorter spans; HV cases are reactance-dominated with longer spans.

**Table 1.** Parameter ranges by MV/HV regime (engineering units).

Parameter	MV	HV
Grid voltage $V_{\text{base}}$	10 kV	110 kV
Base power $S_{\text{base}}$	10 MVA	100 MVA
Line length $L$	1–20 km	1–50 km
Series resistance $R'$	0.5–0.6 $\Omega/\text{km}$	0.15–0.2 $\Omega/\text{km}$
Series reactance $X'$	0.3–0.35 $\Omega/\text{km}$	0.35–0.45 $\Omega/\text{km}$
Shunt capacitance $C'$	8–14 nF/km	8–10 nF/km
Active power $P$	$[-5, 5]$ MW	$[-300, 300]$ MW
Reactive power $Q$	$[-2, 2]$ MVar	$[-150, 150]$ MVar

### 4. EXPERIMENTS AND RESULTS

#### 4.1. Data Preprocessing and Implementation Details

In synthetic grids, extreme draws such as values near the limits of the range, can yield implausible voltages even when NR converges. We therefore remove outliers with a Tukey interquartile-range filter [32] applied to bus-voltage magnitudes in per unit from the NR reference; samples outside  $[Q_1 - 1.5 \text{ IQR}, Q_3 + 1.5 \text{ IQR}]$  are discarded. After filtering, all quantities are converted to per unit using regime-dependent bases  $V_{\text{base}}$  and  $S_{\text{base}}$  with  $Y_{\text{base}} = S_{\text{base}}/V_{\text{base}}^2$ . The corpus contains 33,182 HV and 31,500 MV scenarios for  $N = 4$ –32, split 1:1:1 into train, validation, and test.

PIGNN-MLP uses 4 aggregation channels and an update MLP with hidden size 16. PIGNN-Attn uses the same hidden size with 4

attention heads and 1 attention layer per correction step; the remaining settings are identical. Line search uses initial step  $\alpha_0 = 1.0$ , Armijo constant  $c_1 = 10^{-4}$ , shrink factor  $\beta = 0.5$ , and minimum step  $\alpha_{\min} = 5 \times 10^{-2}$ . Per-iteration caps are  $\Delta\theta_{\max} = 0.3$  rad and  $\Delta|V|_{\max} = 10\%$  of the current magnitude, with voltage bounds  $V_{\min} = 0.8$  and  $V_{\max} = 1.2$ . Training is unsupervised with discounted physics loss  $\gamma = 0.9$ ,  $K = 40$  message-passing steps, AdamW with weight decay  $10^{-3}$ , cosine learning-rate annealing from  $10^{-4}$  to  $10^{-6}$  every 20 epochs, and batch size 64 with block-diagonal batching; runs use a single RTX 3070 8 GB GPU and an Intel Core i7-12700 with 12 cores and 20 threads, up to 4.9 GHz. Hyperparameters were selected by a compact grid search that varied aggregation channels at 4, 8, 16, 32; hidden size from 16 to 128; message-passing steps from 10 to 80 in steps of 10; attention heads 4 or 8; attention layers 1 to 4; angle caps 0.3 to 3.14 rad; magnitude caps 10% to 100% of  $V$ ; and two line search variants: steeper decrease with  $\alpha_0 = 1.0$ ,  $c_1 = 10^{-3}$ ,  $\beta = 0.5$ ,  $\alpha_{\min} = 5 \times 10^{-2}$ ; conservative monotone with  $\alpha_0 = 0.5$ ,  $c_1 = 10^{-4}$ ,  $\beta = 0.7$ ,  $\alpha_{\min} = 5 \times 10^{-2}$ . The reported configuration is best by validation physics loss; wall-clock time breaks ties.

## 4.2. Ablation Studies

1. **Aggregator (MLP vs. self-attention).** Across HV, MV, and combined HV+MV cases, the edge-aware PIGNN-Attn consistently achieves lower voltage-magnitude errors than PIGNN-MLP. For angle predictions, PIGNN-MLP may perform slightly better in the unstabilized setting; however, once stabilization mechanisms (step caps and/or line search) are applied, PIGNN-Attn emerges as the overall best performer.
2. **Per-iteration voltage update caps.** Step caps consistently improve voltage-magnitude accuracy but can degrade angle performance in the MLP setting. In contrast, with the Attn, caps are either beneficial or neutral and effectively suppress worst-case deviations. When combined with line search, caps no longer reduce angle accuracy and instead enhance overall robustness.
3. **Backtracking line search (LS).** LS is the primary driver of both accuracy and robustness for both aggregators. On MV cases, Attn+LS achieves the best performance, while on HV and HV+MV cases, Attn with caps+LS is strongest overall. For the MLP, however, adding caps on top of LS provides little benefit and can even slightly degrade angle accuracy.

For HV+MV, using smaller batches improves accuracy, by reducing cross-regime interference from mixed block-diagonal batching. Although trained on  $N = 4$ –32 grids, the model scales effectively to much larger HV grids (e.g., up to  $N = 1024$ ) with comparable RMSE (about  $V \approx 5 \times 10^{-4}$ ,  $\theta \approx 10^\circ$ ).

## 4.3. Throughput

We benchmark our PIGNN, implemented in PyTorch, against a Newton–Raphson baseline coded as an optimized, vectorized NumPy solver with an analytically assembled Jacobian, across HV grid sizes  $N = 4$  to 1024 under two regimes. In the single-scenario regime, one case per  $N$  is solved: PIGNN runs on a GPU with batch size 1, and NR runs on a CPU with one worker. In the multi-scenario regime, 4096 cases per  $N$  are solved: NR uses 20 CPU workers, and PIGNN runs on a single 8 GB GPU with streaming micro-batches that fully utilize device memory without overflow. To avoid thread oversubscription in CPU multiprocessing, BLAS threads are set to one per process. Timings use the hardware and

**Table 2.** Test RMSE of Voltage Magnitude ( $V$ , p.u.) and Angle ( $\theta$ ,  $^\circ$ ) across HV, MV, and HV+MV

Model	HV		MV		HV+MV	
	$V$	$\theta$	$V$	$\theta$	$V$	$\theta$
<i>Base Models</i>						
PIGNN-MLP	6.6e-2	0.62	7.9e-2	0.67	6.9e-2	1.31
PIGNN-Attn	8.0e-3	0.67	1.5e-2	0.63	2.0e-3	1.27
<i>+Voltage Update Caps</i>						
PIGNN-MLP	1.0e-3	8.20	3.9e-2	3.71	2.6e-2	2.88
PIGNN-Attn	5.4e-4	0.16	1.2e-2	0.58	6.0e-3	1.48
<i>+ Line Search</i>						
PIGNN-MLP	5.8e-4	0.26	1.6e-3	1.38	1.9e-3	1.53
PIGNN-Attn	4.6e-4	0.12	<b>5.7e-4</b>	<b>0.34</b>	2.4e-3	1.26
<i>+Voltage Update Caps, Line Search</i>						
PIGNN-MLP	5.4e-4	0.30	1.7e-3	1.45	2.1e-3	1.68
PIGNN-Attn	<b>3.3e-4</b>	<b>0.08</b>	6.4e-4	0.41	<b>1.9e-3</b>	<b>1.14</b>

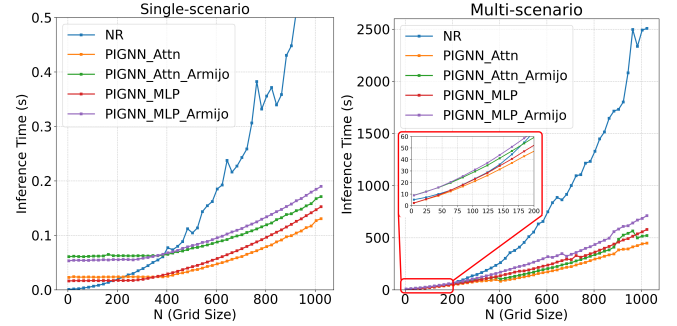


**Fig. 3.** Computational time over grid size for NR and PIGNN variants. Results are reported as median inference time (over multiple runs with 2 warmup and 5 repeat cycles).

software setup described in Section 4.1. Across both regimes, NR time scales super-linearly but polynomially with  $N$  due to sparse factorization and fill-in, while PIGNN grows more gently. In single-scenario runs, NR is competitive for  $N < 200$ , but PIGNN-Attn-LS becomes faster as  $N$  increases; between  $N = 256$  and  $N = 896$  it is about  $2\times$  faster on average, with peak speedups of  $4$ – $5\times$  at the largest grids. In multi-scenario runs, PIGNN-Attn-LS achieves about  $3\times$  higher throughput than NR on average and is consistently faster across all grid sizes.

## 5. CONCLUSION

This work advances AC power-flow solvers by introducing a physics-informed GNN with node/edge physics injection, edge-aware attention, and a line-search-based globalized correction operator, trained without Newton–Raphson supervision. The model achieves NR-level accuracy, and delivers substantial inference speedups. These results highlight the promise of neural-network-based solvers for power systems and motivate future work on broader scalability, rigorous benchmarking, and integration into operational systems.

## 6. REFERENCES

- [1] Attia A. El-Fergany, "Reviews on load flow methods in electric distribution networks," *Archives of Computational Methods in Engineering*, vol. 32, pp. 1619–1633, 2025, Published online Oct. 17, 2024.
- [2] J. Kyle Skolfield and Adolfo R. Escobedo, "Operations research in optimal power flow: A guide to recent and emerging methodologies and applications," *European Journal of Operational Research*, vol. 300, no. 2, pp. 387–404, 2022.
- [3] Engidaw Abel Hailu, George Nyauma Nyakoe, and Christopher Maina Muriithi, "Techniques of power system static security assessment and improvement: A literature survey," *Heliyon*, vol. 9, no. 3, pp. e14524, 2023.
- [4] William F. Tinney and Clifford E. Hart, "Power flow solution by newton's method," *IEEE Transactions on Power Apparatus and Systems*, vol. PAS-86, no. 11, pp. 1449–1460, 1967.
- [5] B. Stott and O. Alsac, "Fast decoupled load flow," *IEEE Transactions on Power Apparatus and Systems*, vol. PAS-93, no. 3, pp. 859–869, 1974.
- [6] W.F. Tinney and J.W. Walker, "Direct solutions of sparse network equations by optimally ordered triangular factorization," *Proceedings of the IEEE*, vol. 55, no. 11, pp. 1801–1809, 1967.
- [7] Azad Deihim, Dimitra Apostolopoulou, and Eduardo Alonso, "Initial estimate of ac optimal power flow with graph neural networks," *Electric Power Systems Research*, vol. 234, pp. 110782, 2024.
- [8] Balthazar Donon, Rémy Clément, Benjamin Donnot, Antoine Marot, Isabelle Guyon, and Marc Schoenauer, "Neural networks for power flow: Graph neural solver," *Electric Power Systems Research*, vol. 189, pp. 106547, 2020.
- [9] Luis Böttcher, Hinrikus Wolf, et al., "Solving ac power flow with graph neural networks under realistic constraints," 2023, pp. 1–7.
- [10] Steven de Jongh, Frederik Gielnik, Felicitas Mueller, Loris Schmit, Michael Suriyah, and Thomas Leibfried, "Physics-informed geometric deep learning for inference tasks in power systems," *Electric Power Systems Research*, vol. 211, pp. 108362, 2022.
- [11] Nan Lin, Stavros Orfanoudakis, Nathan Ordonez Cardenas, Juan S. Giraldo, and Pedro P. Vergara, "Powerflownet: Power flow approximation using message passing graph neural networks," *International Journal of Electrical Power & Energy Systems*, vol. 160, pp. 110112, 2024.
- [12] Sam Yang, Bjorn Vaagensmith, Deepika Patra, Ryan Hruska, and Tyler Phillips, "Multi-fidelity power flow solver," in *2022 Resilience Week (RWS)*, 2022, pp. 1–6.
- [13] Tania B. Lopez-Garcia and José A. Domínguez-Navarro, "Power flow analysis via typed graph neural networks," *Engineering Applications of Artificial Intelligence*, vol. 117, pp. 105567, 2023.
- [14] Damian Owerko, Fernando Gama, and Alejandro Ribeiro, "Optimal power flow using graph neural networks," in *ICASSP 2020 - 2020 IEEE International Conference on Acoustics, Speech and Signal Processing (ICASSP)*, 2020, pp. 5930–5934.
- [15] Xinyue Hu, Haoji Hu, Saurabh Verma, and Zhi-Li Zhang, "Physics-guided deep neural networks for power flow analysis," *IEEE Transactions on Power Systems*, vol. 36, no. 3, pp. 2082–2092, 2021.
- [16] Mei Yang, Gao Qiu, Yong Wu, Junyong Liu, Nina Dai, Yue Shui, Kai Liu, and Lijie Ding, "Physics-guided graph neural networks for real-time ac/dc power flow analysis," 2023.
- [17] Frederik Diehl, "Warm-starting ac optimal power flow with graph neural networks," in *NeurIPS 2019 Workshop on Tackling Climate Change with Machine Learning*, 2019.
- [18] Shengyuan Yan et al., "Data driven approach towards more efficient newton-raphson power flow calculation for distribution grids," 2025.
- [19] Xiao Hu et al., "Adaptive power flow analysis for power system operation based on graph deep learning," *International Journal of Electrical Power & Energy Systems*, vol. 161, pp. 110166, 2024.
- [20] Ashkan B. Jeddi and Abdollah Shafieezadeh, "A physics-informed graph attention-based approach for power flow analysis," in *2021 20th IEEE International Conference on Machine Learning and Applications (ICMLA)*, 2021, pp. 1634–1640.
- [21] Larry Armijo, "Minimization of functions having lipschitz continuous first partial derivatives," *Pacific Journal of Mathematics*, vol. 16, pp. 1–3, 1966.
- [22] Sean Lovett et al., "OPFdata: Large-scale datasets for ac optimal power flow with topological perturbations," 2024.
- [23] Anvita Bhagavathula, Alvaro Carbonero, Ana Rivera, and Priya Danti, "PF $\Delta$ : A benchmark dataset for power flow with load, generator, & topology variations," in *ICLR 2025 Workshop on Tackling Climate Change with Machine Learning*, 2025.
- [24] Hendrik F. Hamann et al., "Foundation models for the electric power grid," *Joule*, vol. 8, no. 12, pp. 3245–3258, 2024.
- [25] Timon Conrad, "AI-based static voltage stability analysis of power grids," 2024.
- [26] Zaheer et al., "Deep sets," in *Advances in Neural Information Processing Systems*, I. Guyon, U. Von Luxburg, S. Bengio, H. Wallach, R. Fergus, S. Vishwanathan, and R. Garnett, Eds. 2017, vol. 30, Curran Associates, Inc.
- [27] Ashish Vaswani et al., "Attention is all you need," in *Advances in Neural Information Processing Systems*, I. Guyon, U. Von Luxburg, S. Bengio, H. Wallach, R. Fergus, S. Vishwanathan, and R. Garnett, Eds. 2017, vol. 30, Curran Associates, Inc.
- [28] Petar Veličković, Guillem Cucurull, Arantxa Casanova, Adriana Romero, Pietro Liò, and Yoshua Bengio, "Graph attention networks," in *International Conference on Learning Representations*, 2018.
- [29] B. R. Oswald, *Vorlesung Elektrische Energieversorgung: Vorlesungsskript*, Eigenverlag / Hochschule (nicht offiziell veröffentlicht), 2005, Korrigierte Ausgabe.
- [30] Z. Kremens and T. Sobierajski, *Analiza systemów elektroenergetycznych (Analysis of Electro Energy Systems)*, Wydawnictwa Naukowo-Techniczne, Warsaw, 1996.
- [31] G. Theil, "Statische stabilität von stromnetzen - erfahrungen bei analyse realer systeme," in *Alternativen für die Energiezukunft Europas*, pp. 1–10, 2012.
- [32] John W. Tukey, *Exploratory Data Analysis*, Addison-Wesley, Reading, MA, 1977.